Soft Matter

Fabrication of Polymer and Carbon Polyhedra Through Controlled Cross-linking and Capillary Deformations

Journal:	*Soft Matter*
Manuscript ID	SM-COM-07-2019-001410.R2
Article Type:	Communication
Date Submitted by the Author:	26-Oct-2019
Complete List of Authors:	George, Derosh; University of California Irvine, Mechanical and Aerospace Engineering Peraza Hernandez, Edwin; University of California Irvine, Mechanical and Aerospace Engineering Lo, Roger; California State University Long Beach, Chemical Engineering Madou, Marc; University of California Irvine, Mechanical and Aerospace Engineering

COMMUNICATION

Fabrication of Polymer and Carbon Polyhedra Through Controlled Cross-linking and Capillary Deformations

Derosh George[a], Edwin A. Peraza Hernandez[a], Roger C. Lo[b], and Marc Madou[a]*

Received 00th January 20xx,
Accepted 00th January 20xx

DOI: 10.1039/x0xx00000x

Fabrication of polymer polyhedral structures is achieved by first producing origami sheets with dissimilar stiffness levels at their folds and faces via multi-step photolithography. Subsequent capillary folding of the sheets towards permanently folded target shapes is realized by thermally controlling, simultaneously, the compliance of the sheets and the volume of the deposited droplets. This fabrication method allows us to create millimeter and sub-millimeter polyhedral structures with arbitrary levels of folding, to manufacture permanently folded polymer polyhedra using single-material monolayer sheets, and to produce carbon shapes from these carbon-rich polymer polyhedra through pyrolysis.

Origami is a technique used to create three-dimensional structures from initially planar sheets by *folding*. It is employed in the design of reconfigurable systems (1–4) and, as reported in this journal, in the fabrication of complex polymer-based structures (5–8). If applied at the the millimeter and submillimeter scales, origami holds promise as a novel fabrication method to produce intricate three-dimensional shapes with unique properties and functionalities (9). To generate folding in origami structures at the submillimeter scale, forces that scale favorably at such length domains must be considered. Different physical forces become more or less dominant depending on their nature as length scales become smaller. *Surface tension* effects become much more dominant at small length-scales. Forces due to surface tension are proportional to the characteristic length of the structure L, while gravity and inertial forces scale with the characteristic volume L^3. For this reason, folding of two-dimensional structures driven by surface tension phenomena has been touted as a potential microfabrication technique (10,11).
Surface tension finds applications in technical areas such as micro- and nano-assembly (12), and fabrication of microlens (13) and nanofilms (14). Investigations on the interactions between liquid and solid substrates reveal that surface tension can induce deformation of soft polymer structures through a fluid-structure interaction known as *elastocapillarity* (15–17). Soft elastomer sheets have been morphed into three-dimensional shapes through elastocapillarity in a process reminiscent of origami folding (10,18–20). However, previous works on elastocapillary-based origami using elastomers succeeded only in producing three-dimensional folded structures that return to their initial flat form when the driving force that folded them (the surface tension of the liquid) is removed (19). While capillary origami and other reversible folding techniques such as those based on swelling (21,22), thermal expansion (6,8,23) or shape memory (24) may lead to a wide variety of applications (25–30), a folding method that allows manufacturing of permanently folded origami shapes in a batch mode would make for a powerful new fabrication method for submillimeter structures. Various strategies have been developed to make permanently folded three-dimensional shapes. Melting and re-solidifying of solder or polymers at the fold regions were used to fabricate permanently folded origami (31–36). In other approaches, the relaxation of pre-stressed films at elevated temperature was used to achieve three-dimensional shapes (12,37). However, these methods demand multi-layer lithography involving more than one material. In contrast, the introduction of differential material properties within a single-layer sheet can reduce the complexity involved in the fabrication process. Different material properties can be introduced across the planform of a photopolymer sheet through selective UV exposure. In a related study, high degree of porosity that was generated by extensively developing a less crosslinked region was used for reversible folding of differentially exposed photopolymer sheets through solvent exchange (38).

Current elastocapillary-based millimeter and submillimeter origami fabrication methods have limitations such as:

1) The requirement for multi-layer lithography involving multiple materials,

[a] *Mechanical and Aerospace Engineering, University of California, Irvine, USA, 92697.*
[b] *Chemical Engineering, California State University, Long Beach, USA, 90840.*
**E-mail: mmadou@uci.edu*
†Electronic Supplementary Information (ESI) available: DOI

2) Inability to control the level of elastocapillary folding (e. g., fold angles) and to lock the structures at desired configurations, and
3) Inability to extend the fabrication methods to materials beyond polymers, such as mechanically, electrically, and electrochemically important materials like carbon.

In this work, we develop and demonstrate an *origami-based fabrication method for three-dimensional structures* of millimeter and submillimeter characteristic lengths obtained by combining lithography, softening and hardening controlled via heat treatment, and elastocapillarity. The present study provides the following contributions to existing capillary origami methods:

1) A *single-layer fabrication route* for a patterned sheet having localized control over the material properties of the faces and folds by using photolithography,
2) *Permanent folding* of the precursor polymer sheets to *the desired target level of folding* (fold angles) by thermally controlling the degree of cross-linking and adjusting the volume of the driving liquid droplet, and
3) A strategy for fabricating *three-dimensional carbon shapes* by ensuring the retention of the polymer shapes during a pyrolysis process.

SU8, a commonly used photopolymer, is used as the base material to fabricate three-dimensional polyhedra. Using a *multi-step* UV exposure photolithography process, a batch fabrication of sheets with a desired fold pattern and localized compliance at the folds and faces is obtained as illustrated in Fig. 1(**a**) (details of the experimental methods are given in the Supplementary Document **A**, ESI†). When the sheets are exposed to UV light, photoacid is generated in the SU8 matrix proportionally to the energy density of the irradiation. The post-exposure bake (PEB) causes cross-linking of the polymer at a rate proportional to the concentration of the photoacid generated in the sheet. By using lithographic photomasks with different uncovered regions, the *first UV exposure* is applied simultaneously to the fold *and* face regions while the *second UV exposure* is applied *only* at the face regions. These two steps allow us to produce less cross-linked compliant folds (where deformation is to be maximized) and more cross-linked stiff faces (where deformation is to be minimized) while the non-exposed SU8 surplus gets completely removed. These characteristics are required to have good agreement with theoretical models of origami. If the two exposure energy densities are less than what is required for complete cross-linking, the patterned sheets *can be released from the supporting structure*.

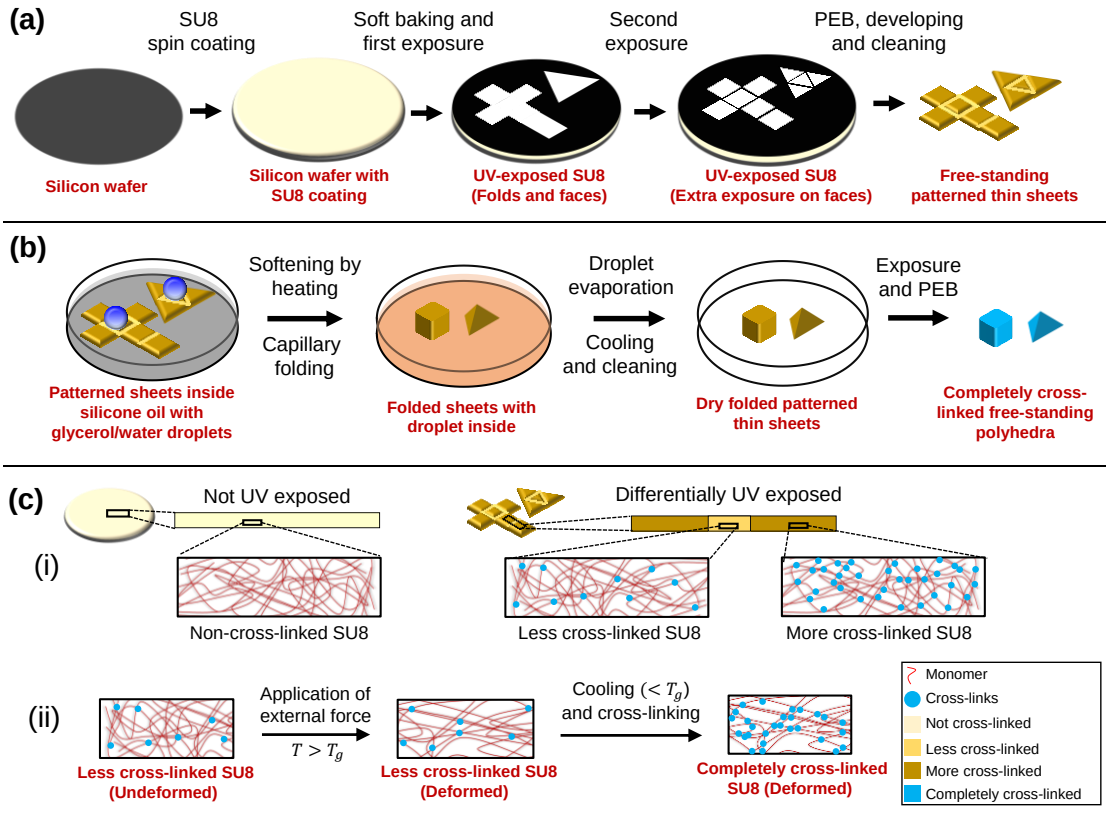

Fig. 1. (**a**) *Photolithography-based patterning of planar thin sheets* used to fabricate free-standing polyhedra. (**b**) *Capillary folding and thermally-controlled softening/hardening*. The sheets are placed inside a silicone oil bath, and actuating droplets are deposited on top of them. The bath is heated to generate thermally-induced softening at the folds and allow folding deformations. The bath is then cooled to acquire permanently folded shapes. (**c**) Schematic of the process at a microstructural level. (i) The degree of cross-linking in the SU8 polymer matrix is directly proportional to the exposure energy. (ii) The less cross-linked regions (the folds) are subjected to significant deformation when external forces are applied, due to the higher mobility of the partially cross-linked monomers. Deformation is made permanent by cooling and subsequently completing the cross-linking of the structures.

After fabrication of the free-standing sheets with different properties at the folds and faces, we proceed to their *folding process* using a combination of elastocapillary bending of the folds induced by a deposited liquid droplet and thermally controlled softening and hardening. *Elastocapillary bending* occurs if the characteristic planform length of the sheet L is in the order of, or larger than, the *elastocapillary length* L_{EC} (i.e., if $L \gtrsim L_{EC} = (Et^3/24(1-\nu^2)\gamma)^{1/2}$, where E, ν, and t are the modulus, Poisson's ratio, and thickness of the sheet, respectively, and γ is the interfacial tension of the liquid droplet) (39). Using dimensions $L = 1$ mm and $t = 50$ µm (representative of the current study), $\nu = 0.5$, and $\gamma = 0.072$ N/m (surface tension of water), the previous inequality demands a modulus $E \lesssim 14.4$ MPa. At room temperature, highly cross-linked SU8 sheets have a modulus in the order of ~2 GPa, significantly above the upper limit requirement (40). Therefore, *unstiffening* of the patterned sheets is required to allow for their capillary folding into three-dimensional shapes (Figs. 1(**b**) and (**c**)). This unstiffening is induced by introducing low density of crosslinking at the folds and by heating the sheets. By doing so, the patterned sheets become more pliable. Dynamic mechanical analysis (DMA) of SU8 strips (2.5 mm × 25 mm × 0.055 mm) was used to characterize the effect of UV exposure time and temperature on their stiffness. DMA analyses were carried out on specimens that were exposed to 40 sec, 60 sec, 80 sec, 100 sec and 180 sec of collimated UV light (2mW/cm^2). In the DMA experiments, temperature was varied from 40°C to 90°C at a ramp rate of 3°C/min. The sample with 180 sec exposure was further subjected to a 2-hour hard bake at 200°C to get complete crosslinking. The results show that the storage modulus (the dynamic modulus that represents the elastic behavior of the material) correlates directly with the exposure energy (Fig. 2(**a**) and Supplementary Document **B**). This correlation indicates a direct relationship between the exposure energy and the cross-linking density (41). Also, as temperature increases, the modulus shows a significant decline as shown in Fig. 2(**a**) for all different exposure times. The less UV exposed sheets exhibit lower modulus values at any given temperature. This difference in stiffness is attributed to the difference in their molecular mobility due to their dissimilar level of cross-linking density (42,43). For the experiments reported here, softening at the folds is induced at 110°C. DMA instrument limitations did not allow us to perform modulus measurements at temperatures above 90°C because of the high softening of the sheets at these temperatures. In view of this limitation, we performed curve-fitting of the obtained data from Fig. 2(**a**) to extrapolate the value of the storage modulus at 110°C. Details on the measurement limitations at temperatures above 90°C and on the extrapolation procedure are provided in Supplementary Document **A**. The extrapolated values of storage modulus at 110°C are 0.38 MPa, 0.74 MPa,

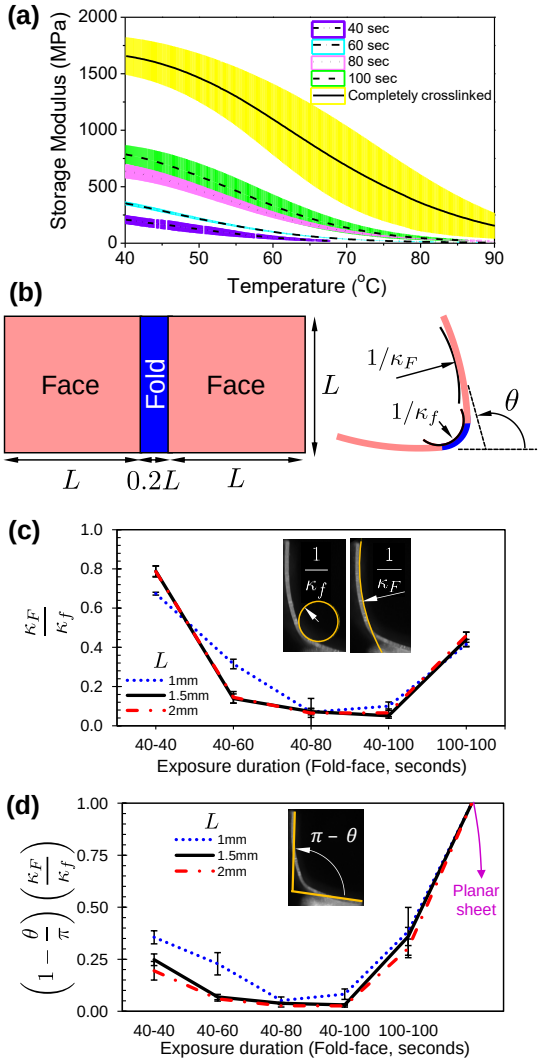

Fig. 2. (**a**) Effect of temperature on the storage modulus of SU8 films made with different UV exposure durations. (**b**) Dimensions of the single-fold sheets and geometric parameters of the folded configurations. (**c**) Effect of exposure times on the ratio of curvature of faces κ_F to curvature of folds κ_f. A 2 mW/cm^2 UV light source is used in all cases. (**d**) Effect of exposure times on the folding parameter that combines fold angle and curvature ratio.

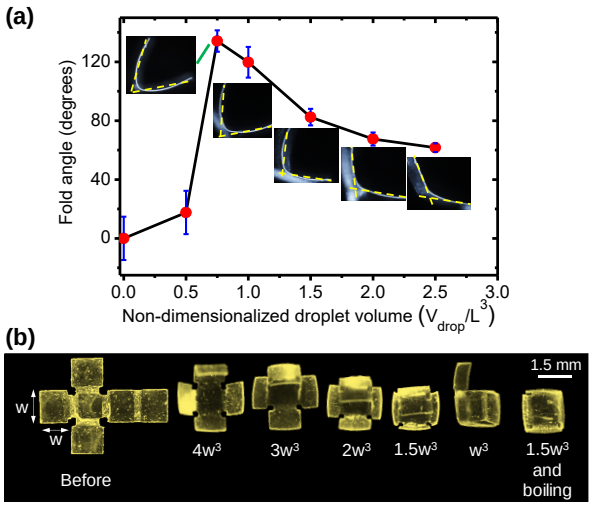

Fig. 3. (**a**) Effect of droplet volume on the fold angle. Single-fold sheets with L = 2 mm are studied (refer Fig. 2(**b**)). (**b**) Effect of droplet volume on the closing of a cube.

2.83 MPa, 2.87 MPa and 33.58 MPa for samples with 40 s, 60 s, 80 s, 100 s, and 180 s (completely crosslinked sample) UV exposure durations, respectively. Note that for all the samples, except the completely crosslinked one, the extrapolated modulus at 110°C is below the estimated threshold value of 14.4 MPa calculated before. The sheets regain their stiffness when they are brought back to their glassy state by cooling them to room temperature.

Folding of the thermally unstiffened sheets (with their temperature elevated to 110°C) is triggered by placing a liquid droplet on top of them as shown in Fig. 1(**b**) and Movie **S1** (ESI†). To minimize the energy of the sheet-droplet system, i.e., the addition of the sheet strain energy and the droplet surface energy, the sheet is deformed towards a shape that aims to enclose the droplet. The obtained folded sheet accurately resembles the targeted three-dimensional origami polyhedron due to the differential compliance between folds and faces. Two additional observations were made on this process: *i*) In the absence of a droplet, heating the sheets does not induce discernable folding, suggesting that cross-linking gradients across the sheet thickness caused during the photolithography process are negligible; and *ii*) Heating the patterned sheets for an hour or more (i.e., an extended PEB that induces a high level of cross-linking in the sheets) prior to placing a droplet on top of them results in negligible folding deformation (Supplementary Fig. **SA1** and Movie **S2,** ESI†). The latter observation suggests that a high level of cross-linking in the sheets hinders the capillary deformation because of the resulting high stiffness.

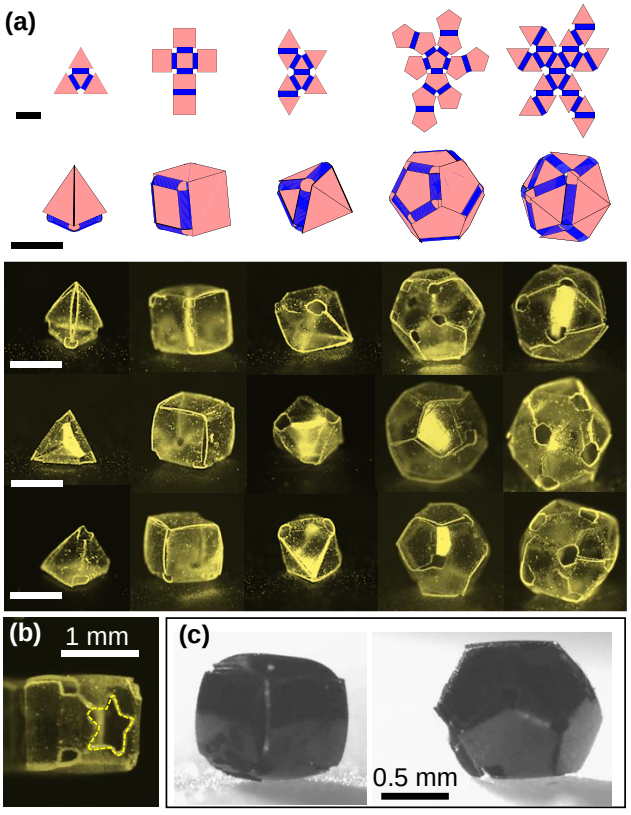

Fig. 4. (**a**) Platonic polyhedra obtained using the present fabrication method. The scale bars are 1.5 mm long. (**c**) Cube with a star-shaped hole on one of its faces. (**b**) Carbon origami cube and dodecahedron produced from corresponding polymer shapes.

To select favorable exposure times for the two-step UV exposure photolithography process considering a specified sheet thickness (55±3 μm here), a quantitative study on the influence of the exposure times on the resulting folded geometry was performed (Supplementary Fig. **SA2** and Table **SA1** provide raw data of this study, ESI†). Rectangular sheets with a centered single fold were experimentally analyzed. The geometry of the sheets and parameters of interest (*fold angle* (θ), *curvatures of the faces* (κ_F) and *folds* (κ_f)) are illustrated in Fig. 2(**b**). Figure 2(**c**) shows that the ratio of the curvature of the faces (κ_F) to the curvature of the fold (κ_f) decreases as the exposure time of the faces is increased with respect to that of the folds. A low value for this ratio allows for better agreement with theoretical models for origami (where faces are rigid and folds are highly flexible).

The quality of the folding deformation of the sheets was also quantified by a *folding parameter* defined as $(\kappa_F/\kappa_f)(1-\theta/\pi)$. A smaller folding parameter indicates more favorable folding deformation (with large fold angle and low face-to-fold curvature ratio). As shown in Fig. 2(**d**), fold-face exposure times of 40-80 sec and 40-100 sec exhibited better folding quality as quantified by the folding parameter. Based on these results, it was opted to use exposure times of 40-80 sec for all subsequent experiments. Such exposure times were selected because it was observed that 40-100 sec exposure times often led to sheet breakage at the folds during the SU8 development step. The sheets made by exposing the folds for 40 sec and the faces for 80 sec showed no detachment of the faces from the folds. However, cracks could appear at some folds if the development is performed with stirring. Although we abstained from using a stirrer for the development, unintentional disturbances introduced while handling the sheet-laden liquid caused some defects. More fine tuning of the process is required to avoid this issue completely.

The volume of the actuating droplet also affects the capillary folding deformation. To quantify this, we performed

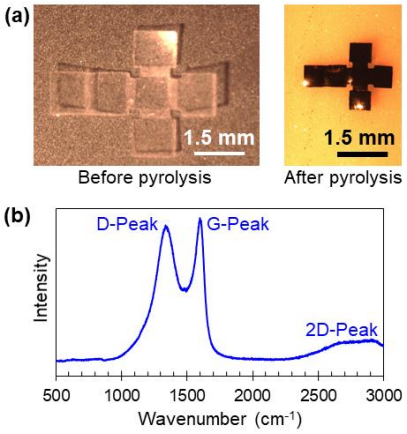

Fig. 5. (**a**) Size comparison of sheets before and after pyrolysis. (**b**) Raman spectroscopy of the carbonized SU8 origami polyhedra showing the D-peak, the G-peak and the 2D-peak.

experiments on single-fold sheets and cube sheets using different droplet volumes. Figure 3(**a**) shows fold angle vs. droplet volume for the single fold sheets. From the considered droplet volumes V_{drop}, $0.75L^3$ exhibited the largest folding angle. Droplet volumes below $0.75L^3$ produced smaller folding angles due to their lower surface energy and smaller contact area with the sheet. Droplet volumes above $0.75L^3$ also produced smaller folding angles. Although these larger droplets possess higher surface energy, the size of the droplets themselves constrain the folding deformation of the sheet.

The effect of droplet volume on the folding response is also studied by folding cube sheets (Fig. 3(**b**)). The results show that droplet volumes larger than the target polyhedral volume do not allow the sheets to completely fold into their target closed polyhedron (Fig. 3(**b**)). To overcome the aforementioned issues, a droplet with volume larger than the target polyhedral volume (1.5 times larger in the examples shown here) was initially deposited to ensure that the droplet comes in contact with all the faces of the sheet as it folds. Afterward, the surplus liquid is gradually removed by boiling the water droplet. This process allowed to produce fully closed origami polyhedra. The obtained polymer polyhedra showed good agreement with the anticipated polyhedral shapes with smooth folds from theoretical simulations (20) as shown in Fig. 4(**a**). Furthermore, folded sheets with any intermediate fold angle configurations between the flat and the fully closed polyhedron configurations can be fabricated by stopping the heat application and cooling the sheet when it has reached the targeted intermediate shape.

A variation that allows for the formation of *hole cut-outs* inside the faces of the sheets was also explored. Hole cut-outs inside the faces are introduced by using lithographic photomasks that do not expose the cut-out regions to UV irradiation at any step. When folded, the sheets having faces with hole cut-outs can form three-dimensional structures with patterned walls (Fig. 4(**b**)). Additionally, the precursor sheets can be kept anchored to the supporting structure instead of being free-standing by introducing a third exposure to the anchor region (see Supplementary Fig. **SA3,** ESI†).

Structures formed by completely cross-linked SU8, a polymer with high carbon content, can be converted into corresponding isometrically shrunken carbon shapes through pyrolysis (44). To demonstrate this, folded polyhedra are first subjected to flood UV exposure to complete the cross-linking at the folds and the faces. This complete cross-linking ensures that the folded shapes obtained using capillary origami retain their form during pyrolysis. Results of carbonized shapes obtained from corresponding polymer shapes are shown in Fig. 4(**c**). The original polymer polyhedral shapes were preserved in the corresponding carbon shapes. Comparison of the sizes of the polymer shapes before and after pyrolysis show that the polymer origami structures were shrunk isometrically by about 57% of their original size when converted into carbon (Fig. 5(**a**)). The microstructural characterization of the carbon polyhedra obtained from the polymer polyhedra was performed using Raman spectroscopy (Fig. 5(**b**)). The ratio of the intensities of the D-peak (at 1350 cm^{-1}) to that of the G-peak (at 1550 cm^{-1}) obtained here is 1.03, and the ratio of the 2D-peak (2690 cm^{-1}) to the G-peak intensity is 0.12. These ratios indicate the formation of carbon structures that are glassy in nature (45). These carbon shapes can be metalized using techniques such as electroless deposition and electroplating to create origami structures formed by different materials (46).

Conclusions

We have presented an origami-based method for fabricating polymer three-dimensional polyhedra. By using a single-layer photopolymer and by modulating the energy applied in different UV exposure steps, folds and faces with different localized stiffness can be created. The employed actuation mechanism is based on a combination capillary forces and controlled thermal softening/stiffening. The process allows for the creation of origami structures that are *permanently locked* in their target polyhedral shapes. Since the procedure is based on photolithography, it is a batch process that is scalable in terms of size and number of the simultaneously fabricated structures. Arbitrarily-shaped hole cut-outs at the faces can also be introduced in the photolithography process. Furthermore, the polymer polyhedra can be converted to carbon through pyrolysis. These carbon polyhedra open a plethora of routes to make submillimeter structures with different material and surface properties. The potential applications of the fabricated structures include drug encapsulation and delivery capsules, packages for sensors and systems, plasmonic devices, among others.

Conflicts of interest

There are no conflicts to declare.

Acknowledgements

This work was funded in part by the National Science Foundation (NSF) grant #1449397. The assistance from Loan Le in the preliminary experimental work is acknowledged. The authors thank the UCI Laser Spectroscopy labs for access to their Raman spectroscopy equipment. DMA analysis was performed at the UC Irvine Materials Research Institute (IMRI). D.G. is partially funded by the Science and Engineering Research Board (SERB), India. E.P.H. acknowledges the start-up support from the Department of Mechanical and Aerospace Engineering at the University of California, Irvine.

References

1. Miyashita S, Guitron S, Li S, Rus D. Robotic metamorphosis by origami exoskeletons. Sci Robot. 2017;4369(2):1–7.
2. McGuire T, Hirsch M, Parsons M, Leake S, Straub J. A CubeSat deployable solar panel system. Energy Harvest Storage Mater Devices, Appl VII. 2016;9865(May):98650C.

3. Tang R, Huang H, Tu H, Liang H, Liang M, Song Z, et al. Origami-enabled deformable silicon solar cells. Appl Phys Lett. 2014;104(8).
4. Mikulas M, Pappa R, Warren J, Rose G. Telescoping solar array concept for achieving high packaging efficiency. Am Inst Aeronaut Astronaut 1. 2015;AIAA 2015-:1–21.
5. Felton SM, Tolley MT, Shin B, Onal CD, Demaine ED, Rus D, et al. Self-folding with shape memory composites. Soft Matter. 2013;9(32):7688–7694.
6. Dickey MD, Liu Y, Boyles JK, Genzer J, Dickey MD. Self-folding of polymer sheets using local light absorption. Soft Matter. 2012;8(6):1703–2044.
7. Ionov L. Soft microorigami: self-folding polymer films. Soft Matter. 2011;7(15):6786–91.
8. Cui J, Yao S, Huang Q, Adams JGM, Zhu Y. Controlling the self-folding of a polymer sheet using a local heater: The effect of the polymer-heater interface. Soft Matter. 2017;13(21):3863–70.
9. Rogers J, Huang Y, Schmidt OG, Gracias DH. Origami MEMS and NEMS. MRS Bull. 2016;41(2):123–9.
10. Py C, Reverdy P, Doppler L, Bico J, Roman B, Baroud CN. Capillary origami: Spontaneous wrapping of a droplet with an elastic sheet. Phys Rev Lett. 2007;98(15):2–5.
11. Van Honschoten JW, Berenschot JW, Ondacuhu T, Sanders RGP, Sundaram J, Elwenspoek M, et al. Elastocapillary fabrication of three-dimensional microstructures. Appl Phys Lett. 2010;97(1).
12. Boncheva M, Whitesides GM. Templated self-assembly: Formation of folded structures by relaxation of pre-stressed, planar tapes. Adv Mater. 2005;17(5):553–7.
13. Damodara S, George D, Sen AK. Single step fabrication and characterization of PDMS micro lens and its use in optocapillary flow manipulation. Sensors Actuators, B Chem. 2016;227:383–92.
14. Hu L, Chen M, Fang X, Wu L. Oil-water interfacial self-assembly: A novel strategy for nanofilm and nanodevice fabrication. Chem Soc Rev. 2012;41(3):1350–62.
15. Style RW, Che Y, Park SJ, Weon BM, Je JH, Hyland C, et al. Patterning droplets with durotaxis. Proc Natl Acad Sci U S A. 2013;110(31):12541–4.
16. van Honschoten JW, Escalante M, Tas NR, Elwenspoek M. Formation of liquid menisci in flexible nanochannels. J Colloid Interface Sci. 2009;329(1):133–9.
17. Kim H-Y, Mahadevan L. Capillary rise between elastic sheets. J Fluid Mech. 2006;548:141.
18. Piñeirua M, Bico J, Roman B. Capillary origami controlled by an electric field. Soft Matter. 2010;6:4491.
19. Geraldi NR, Ouali FF, Morris RH, McHale G, Newton MI. Capillary origami and superhydrophobic membrane surfaces. Appl Phys Lett. 2013;102(21).
20. Hernandez EAP, Hartl DJ, Lagoudas DC. Active Origami: Modeling, Design, and Applications. Springer; 2018.
21. Ionov L. Biomimetic hydrogel-based actuating systems. Adv Funct Mater. 2013;23(36):4555–70.
22. Rath A, Mathesan S, Ghosh P. Folding behavior and molecular mechanism of cross-linked biopolymer film in response to water. Soft Matter. 2016;12:9210–22.
23. Kobayashi K, Oh SH, Yoon C, Gracias DH. Multitemperature responsive self-folding soft biomimetic structures. Macromol Rapid Commun. 2018;1700692(39):1–7.
24. Mao Y, Yu K, Isakov MS, Wu J, Dunn ML, Qi HJ. Sequential self-folding structures by 3D printed digital shape memory polymers. Sci Rep. 2015;13616(5):1–12.
25. Peraza Hernandez EA, Hartl DJ, Malak Jr RJ, Lagoudas DC. Origami-inspired active structures : a synthesis and review. Smart Mater Struct. 2014;94001(23):1–28.
26. George D, Anoop R, Sen AK. Elastocapillary powered manipulation of liquid plug in microchannels. Appl Phys Lett. 2015;107(26):261601.
27. Samy RA, George D, Sen AK. Bio-inspired liquid transport via elastocapillary interaction of a thin membrane with a liquid meniscus. Soft Matter. 2017;13(38):6858–69.
28. Fernandes R, Gracias DH. Self-folding polymeric containers for encapsulation and delivery of drugs. Adv Drug Deliv Rev. 2012;64(14):1579–89.
29. Na JH, Evans AA, Bae J, Chiappelli MC, Santangelo CD, Lang RJ, et al. Programming reversibly self-folding origami with micropatterned photo-crosslinkable polymer trilayers. Adv Mater. 2015;27(1):79–85.
30. Zhao Z, Wu J, Mu X, Chen H, Qi HJ, Fang D. Origami by frontal photopolymerization. Sci Adv. 2017;1602326(3):1–8.
31. Filipiak DJ, Azam A, Leong TG. Hierarchical self-assembly of complex polyhedral microcontainers. J Micromechanics Microengineering. 2009;75012(19):1–6.
32. Leong TG, Randall CL, Benson BR, Zarafshar AM, Gracias DH. Self-loading lithographically structured microcontainers: 3D patterned, mobile microwells. Lab Chip. 2008;8(10):1621–4.
33. Cho J, Gracias DH. Self-assembly of lithographically patterned nanoparticles. Nano Lett. 2009;9(12):4048–51.
34. Azam A, Laflin KE, Jamal M, Fernandes R, Gracias DH. Self-folding micropatterned polymeric containers. Biomed Microdevices. 2011;13:51–8.
35. Cho JH, James T, Gracias DH. Curving nanostructures using extrinsic stress. Adv Mater. 2010;22(21):2320–4.
36. Gracias DH, Kavthekar V, Love JC, Paul KE, Whitesides GM. Fabrication of micrometer-scale, patterned polyhedra by self-assembly. Adv Mater. 2002;14(3):235–8.
37. Tyagi P, Bassik N, Leong TG, Cho J, Benson BR, Gracias DH. Self-assembly based on chromium / copper bilayers. J Microelectromechanical Syst. 2009;18(4):784–91.
38. Jamal M, Zarafshar AM, Gracias DH. Differentially photo-crosslinked polymers enable self- assembling microfluidics. Nat Commun. 2013;2:527.
39. Bico J, Reyssat É, Roman B. Elastocapillarity: When Surface Tension Deforms Elastic Solids. Annu Rev Fluid Mech. 2017;
40. Wouters K, Puers R. Determining the Young's modulus and creep effects in three different photo definable epoxies for MEMS applications. Sensors Actuators, A Phys. 2009;156(1):196–200.
41. Feng R, Farris RJ. Investigation of thermal and mechanical properties of SU8 negative photoresist coatings. J Micromechanics Microengineering. 2003;13(1):80–88.
42. Hill LW. Paint and coating testing manual, fourteenth edition of the Gardner-Sward handbook. ASTM; 1995. 534-546 p.
43. Mujtaba A, Keller M, Radusch H-J, Thurn-Albrecht T, Saalwächter K, Beiner M. Mechanical properties and cross-link density of styrene − butadiene model composites containing fillers with bimodal particle size distribution. Macromolecules. 2012;45:6504–15.

44. Wang C, Zaouk R, Park BY, Madou MJ. Carbon as a MEMS material: micro and nanofabrication of pyrolysed photoresist carbon. Int J Manuf Technol Manag. 2008 Jan;13(2):360–75.
45. Bukalov SS, Leites LA, Sorokin AI, Kotosonov AS. Structural changes in industrial glassy carbon as a function of heat treatment temperature according Raman spectroscopy and X-ray diffraction data. Nanosyst Physics, Chem Math. 2014;5(1):186–91.
46. Judd NCW. Electroless deposition of copper and nickel on carbon fibres. Composites. 1970;345.

Polymer and carbon polyhedra are fabricated using a novel method that combines photolithography and controlled capillary folding

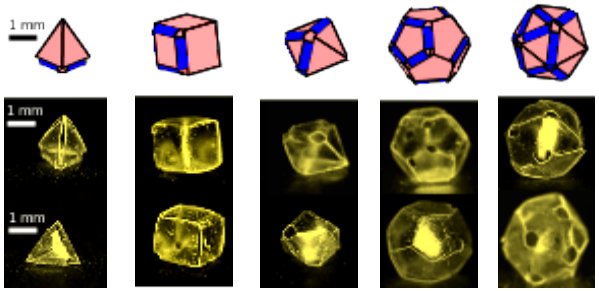
1 mm
1 mm
1 mm